First-principles study of defects and phase transition in UO_2

2009 J. Phys.: Condens. Matter 21 435401

(http://iopscience.iop.org/0953-8984/21/43/435401)

J. Phys.: Condens. Matter **21** (2009) 435401 (10pp) doi:10.1088/0953-8984/21/43/435401

First-principles study of defects and phase transition in UO_2

Jianguo Yu, Ram Devanathan[1] and William J Weber

Pacific Northwest National Laboratory, PO Box 999, Richland, WA 99352, USA

E-mail: ram.devanathan@pnl.gov

Received 9 May 2009, in final form 15 August 2009
Published 5 October 2009
Online at stacks.iop.org/JPhysCM/21/435401

Abstract

Defect properties and phase transition in UO_2 have been studied from first principles by the all-electron projector-augmented-wave (PAW) method. The generalized gradient approximation with empirical self-interaction correction, (GGA) + U, formalism has been used to account for the strong on-site Coulomb repulsion among the localized U 5f electrons. The Hubbard parameter U_{eff}, magnetic ordering, chemical potential and heat of formation have been systematically examined. By choosing an appropriate $U_{\text{eff}} = 3.0$ eV it is possible to consistently describe structural properties of UO_2 and model the phase transition processes. The phase transition pressure for UO_2 is about 20 GPa, which is less than the experimental value of 42 GPa but better than the LDA + U value of 7.8 GPa. Meanwhile our results for the formation energies of intrinsic defects partly confirm earlier calculations for the intrinsic charge neutral defects but reveal large variations depending on the determination of the chemical potential and whether the environment is O-rich or U-rich. Moreover, the results for extrinsic defects of Xe, which are representative of mobile insoluble fission product in UO_2, are consistent with experimental data in which Xe prefers to be trapped by Schottky defects.

(Some figures in this article are in colour only in the electronic version)

1. Introduction

Uranium dioxide (UO_2) is by far the most commonly used nuclear fuel. Its physical, chemical and thermodynamic properties have been studied extensively for over half a century by both experimental and theoretical methods [1]. One of the most important performance metrics for nuclear fuel materials is the fuel rod behaviour under extreme conditions of high temperature, high pressure and high radiation dose. For safe operation, it is crucial to have a fundamental understanding of the fuel mechanical and thermal behaviours under irradiation. Under reactor operating conditions, the fuel rod behaviour is affected by many phenomena, and it is sometimes very difficult to characterize each process individually by experiment [2]. For example in high burnup of the fuel, many microstructural changes take place that are not easy to observe by experiment. Furthermore, in order to develop new types of high burnup fuels, it is essential to develop an atomic-level understanding of fundamental mechanisms governing the degradation of fuel performance. However, only limited experimental studies have been carried out in this area because of either the small length scale or the difficulty in isolating the contribution of specific factors on properties.

Computational modelling and simulation can help overcome the deficiencies of experiment and explore materials properties and performance limitations. For instance, ground state Kohn–Sham density functional theory (DFT) [3] has been successfully applied to determine the properties of defects in solids, especially for metals and semiconductors. Such calculations most frequently rely upon periodic boundary conditions and plane-wave basis sets to simulate bulk materials in the presence of impurities. Although the success of the plane-wave DFT methodology is well proven in predicting the structures of defects and their formation energies in metals and semiconductors, for example III–V semiconductors [4], accurate calculation of defects in ionic insulators, which in general have significantly high values of the heat of formation energy, poses a challenge [5]. Due to the restriction of periodic boundary conditions from which periodic-image errors arise, predicted properties, such as defect formation energy, depend strongly on the subtle details of the actual implementation,

[1] Address for correspondence: Pacific Northwest National Laboratory, MS K8-87, PO Box 999, Richland, WA 99352, USA.

i.e. the finite size of the supercell, the exchange correlation (XC) energy functional and the choice of pseudopotential. Additional complications arise for oxide materials with strongly Coulomb correlated electrons, especially for oxides with partly filled d or f electrons of transition metals, in which the effective Hubbard parameter, U_{eff}, and the magnetic ordering may also strongly influence the results [6].

For UO_2, conventional DFT schemes, such as the local density approximation (LDA) and the generalized gradient approximation (GGA) [7], incorrectly indicate a metallic ground state, which disagrees with available experiments [8]. The discrepancy is due to the approximation for the exchange correlation (XC) energy functional, which yields a qualitatively *incorrect* behaviour for the localized 5f orbital of the uranium atom in UO_2. In order to take into account the localized 5f orbital dependence of the Coulomb and exchange interactions, a rotationally invariant approach, in which a multiorbital mean-field Hubbard term is added to the LDA functional (LDA + U) [9, 10], has been developed. In particular, in this LDA + U approach only the difference ($U_{\text{eff}} = U - J$) between the Coulomb U and exchange J parameters is significant, and the underestimation of the intra-band Coulomb interaction is corrected by the effective Hubbard parameter U_{eff}. This approach is known to reproduce not only ground state properties, such as lattice constant, cohesive energy and bulk modulus, but also excited state properties such as the band gap of UO_2. For example, recent *ab initio* calculations [11] have confirmed the experimental observation [12] that UO_2 in the cubic fluorite ($Fm\bar{3}m$) structure is an antiferromagnet. However, subtle details of the actual implementation can strongly influence the results, i.e. the band gaps and the energies depend on the effective Hubbard U_{eff} parameter, the choice of the localized orbitals (valence or core), the magnetic ordering, the spin–orbital coupling and the underlying exchange correlation functional (LDA or GGA) [13].

In this work we systematically study the bulk properties of UO_2, such as the ground state structural, electronic and magnetic properties, using GGA + U formalism. In particular we focus on constructing a suitable theoretical framework using GGA + U for UO_2 that reflects the correct antiferromagnetic (AF) insulator ground state of a UO_2 crystal by incorporating the effect of strongly correlated 5f electrons in uranium atoms through the Hubbard U_{eff} correction. Meanwhile, the effects of the magnetic ordering and the spin–orbital coupling are also investigated in order to determine structural properties of the UO_2 system.

It is well known that the cubic fluorite phase ($Fm\bar{3}m$) is the ground state structure of UO_2; however, under extreme operating conditions, UO_2 may transform to the high-pressure orthorhombic cotunnite-type structure ($Pnma$). Figure 1 shows the structure of these two phases of UO_2. A recent study, using LDA + U, calculated the phase transition pressure to be 7.8 GPa [14], which is significantly lower than the experimental transition pressure of 42 GPa [15]. In the present work, this phase transition is examined and formation energies of intrinsic defects in UO_2 are calculated using the GGA + U formalism.

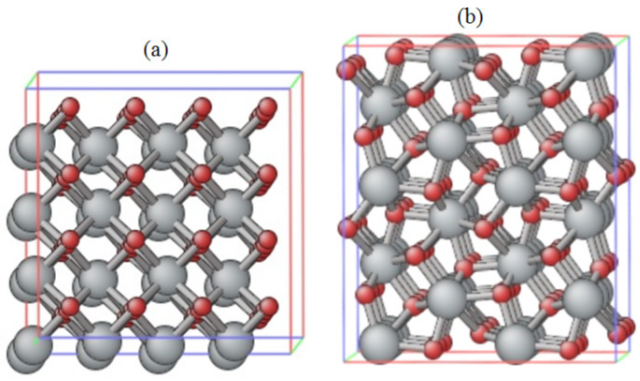

Figure 1. Structure of (a) $Fm\bar{3}m$ and (b) $Pnma$ phases of UO_2.

In this paper we also attempt to calculate accurately the defect formation energies of uranium dioxide (UO_2) in the fluorite ($Fm\bar{3}m$) structure. Defects are formed during operation by radiation-induced displacement of ions from their lattice sites. As a thermally activated process, intrinsic defect production does not require the addition of impurities. One of the key properties of intrinsic defects is the formation energies, which play a critical role in UO_2 fuel under reactor operating conditions. Moreover, many physical and chemical properties of UO_2 are closely related to the quantum processes associated with localization and delocalization of U 5f electrons. Thus the study of defects in UO_2 may help in understanding the fundamental science of oxide materials with strongly Coulomb correlated electrons, especially for transition metal oxides with partly filled d or f electrons.

A number of previous attempts have been made to determine the formation energies of defects in UO_2. The results vary greatly, even for the charge neutral defect system, depending on the subtle details of the actual implementation of methodologies [16–20]. For example, the formation energy of a neutral oxygen interstitial has been variously quoted by DFT calculations as −2.9 eV [16], −2.5 eV [17], −1.6 eV [18], −0.44 eV [19] and −1.34 eV [20]. Such variation may be attributed to the use of different approaches for calculating the oxygen chemical potential and different treatments of the problem by DFT.

Fission gas significantly affects the performance of the fuel matrix under operating conditions, as well as the spent fuel matrix in interim storage or in a geological repository [21]. In particular, the presence of rare gases in the fuel matrix can lead to the formation of bubbles and possible swelling and cracking of fuels. The fission gas can also escape to the plenum to increase the pressure on the cladding, which can be burnup-limiting, or can cause cladding rupture. Similar risks exist for containers of spent nuclear fuel under storage conditions. Furthermore, mixing xenon (Xe) fission gas with the helium plenum gas decreases the thermal conductivity of the fuel–cladding gap and can result in fuel overheating. The behaviour of fission gases is thus a key safety issue. For these reasons, the behaviour of fission gases has been the subject of extensive research by both experimental and theoretical methods [22, 23]. Among all fission gases, Xe is representative of mobile insoluble fission products in the

matrix of UO_2. Despite the importance of the behaviour of fission gas in fuels, a detailed atomic understanding of the evolution of fission gas bubbles in fuels and their interaction with the microstructure is lacking. In addition, characterizing the associated phenomena of noble gases in the fuel may help in understanding the evolution of bubbles and nanoparticles embedded in a crystalline matrix. In this study, we calculate the formation energies of Xe in a variety of sites in UO_2 using GGA + U.

2. Calculation method

The DFT calculations described here were performed using the frozen-core all-electron projector-augmented-wave (PAW) [24, 25] method, as implemented in the *ab initio* total energy and molecular dynamics program VASP (Vienna *ab initio* simulation program) [26]. The spin polarization calculations were carried out as a simplification of the complex magnetism in UO_2, whereas spin–orbit interactions were also considered in some cases. To ensure accurate results, a plane-wave cutoff energy of 500 eV was used for all calculations. Gaussian smearing was used with a smearing parameter of 0.20 eV.

Both $Fm\bar{3}m$ and $Pnma$ phases were treated with GGA + U, which is aligned with the LDA + U formalism proposed by Dudarev *et al* [9] to account for the strong on-site Coulomb repulsion among the localized U 5f electrons. The supercell for electronic structure calculations was U_4O_8 for both structures with periodic boundary conditions. The Brillouin-zone integrations were performed using the Monkhorst–Pack grids, and employed (8×8×8) and (6×10×6) meshes for $Fm\bar{3}m$ and $Pnma$, respectively. The equilibrium volume was determined by optimizing all internal structural parameters at constant cell volume and then minimizing the energy with respect to the cell volume. All internal structural parameters were relaxed until the Hellmann–Feynman forces on each ion were negligible (<0.001 eV $Å^{-1}$).

Supercells containing defects were generated by constructing a 2 × 2 × 2 conventional 12-atom unit cell. To avoid spurious elastic interaction with defects in neighbouring supercells, lattice constants were fixed at the theoretical values. Meanwhile impurities were removed or added to sites close to the supercell centre. All atoms except for three atoms far away from the centre of impurity were allowed to relax. A value of 3.0 eV for U_{eff} was used. The Brillouin-zone integrations were performed using the Monkhorst–Pack grids, and (2 × 2 × 2) meshes were employed with an additional shift of mesh by (0.15, 0.15, 0.15) to avoid the Γ point as one of sample points [4]. Two possible magnetic states were studied: antiferromagnetic (AF) and ferromagnetic (FM).

The U metal state was also treated with the GGA + U formalism, and only the results for the α-phase are presented here. The electronic structure calculations for α-U were performed with a four-atom supercell, and the Brillouin-zone integrations employed Monkhorst–Pack grids with (16 × 10 × 10) meshes. The calculation for the O_2 molecule was performed in a cubic box (14×14×14 $Å^3$). For the calculation of the atomization energies, we evaluated the spin-polarized total energy of the free O and U atoms using the same cubic box. For both the U and O atoms, no constraint was imposed on the one-electron occupation.

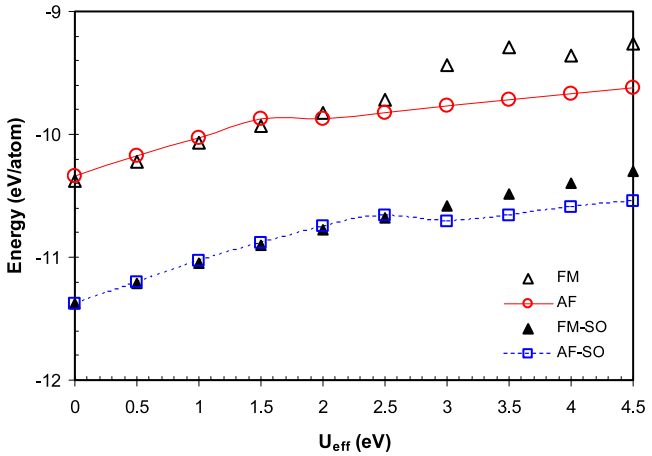

Figure 2. Lattice energy as a function of the effective U_{eff}. Four configurations are considered: antiferromagnetic (AF) and ferromagnetic (FM) with/without spin–orbital coupling.

3. Results and discussion

3.1. Structural properties

In order to choose an appropriate U_{eff} to consistently describe structural properties of UO_2, we calculated the total lattice energies of various magnetic structures with different effective U_{eff} values, and the results are shown in figure 2. Four configurations are discussed here: AF and FM with and without spin–orbital coupling. As shown in figure 2, for each magnetic state, the total lattice energy decreases as the effective U_{eff} increases due to increases in the strength of hybridization for U 5f and O 2p orbitals. If the U 5f orbitals were completely unoccupied, one would expect the total lattice energy to be independent of U_{eff}, as well as the lattice constant a. Meanwhile, the stability of the different configurations depends on the effective U_{eff}. In particular, the AF structure is more stable only if U_{eff} is more than 3.0 eV and 2.0 eV, with and without the spin–orbital coupling, respectively. With the spin–orbital coupling, the total energy for either the AF or FM structure is always below the corresponding counterpart without the effect of the spin–orbital coupling, and the energy difference is 1.0 eV for the effective U_{eff} ranging from 0 to 4.5 eV. This can be interpreted as evidence of magnon–phonon coupling resulting in a strong cohesion of the UO_2 system.

Figure 3 shows the equilibrium relative lattice constants (a/a_0 and c/a_0) as a function of the effective U_{eff}. The lattice constants are given as fractions of the experimental value of $a_0 = 5.468$ Å for four cases: AF/FM with and without spin–orbital coupling. For all four cases, good agreement with experiment is evident in figure 3 based on the fact that the relative lattice constant is within 2% of unity. The lattice parameter in general increases with U_{eff} for UO_2, and the reason for this behaviour is a slight hybridization of U 5f and O 2p orbitals. However, after full relaxation of the supercell, only

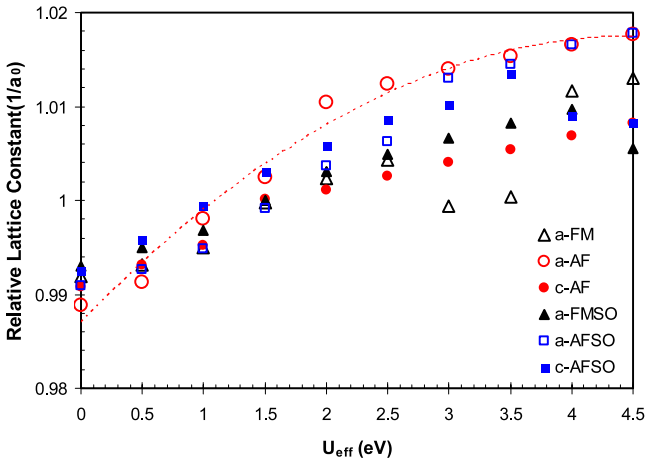

Figure 3. Equilibrium relative lattice constants (a/a_0 and c/a_0) as a function of the effective $U_{\rm eff}$ for four cases: AF/FM with/without spin–orbital coupling. The experimental lattice constant $a_0 = 5.468$ Å. The dotted line is drawn to guide the eye.

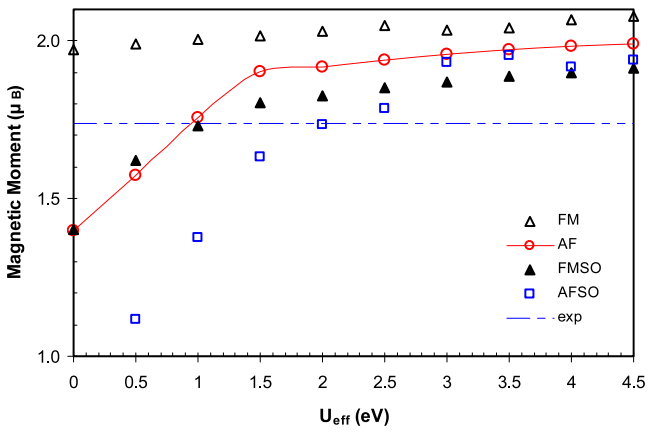

Figure 4. Magnetic moment as a function of the effective $U_{\rm eff}$ from 0 to 4.5 eV for four cases, AF/FM with/out spin–orbital coupling, as well as comparison with the experimental value of 1.74 $\mu_{\rm B}$ (horizontal line).

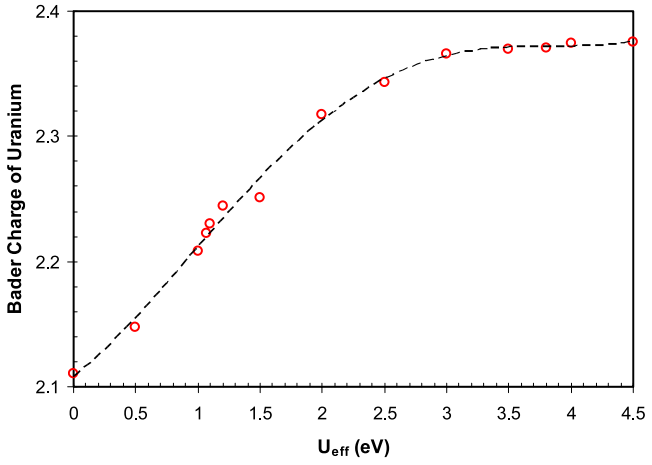

Figure 5. The Bader charge of uranium as a function of the effective $U_{\rm eff}$ from 0 to 4.5 eV for the case of antiferromagnetic configuration.

the FM structure can maintain the cubic lattice either with or without the spin–orbital coupling, and the AF structure shows tetragonal symmetry ($a = b \neq c$) due to the antiferromagnetic ordering along the c-axis [19] In particular, as $U_{\rm eff}$ increases, c changes from $c > a$ to $c < a$ and the corresponding value for $U_{\rm eff}$ depends on whether the effect of the spin–orbital coupling is considered or not. Meanwhile, for $U_{\rm eff} \geqslant 2.0$ eV, the lattice parameter is slightly overestimated for both cases, but the lattice constant difference between a and c is larger for the case without spin–orbital coupling.

In order to gain further insight into the properties of the UO_2 system, we have investigated magnetic properties by taking into account both spin–orbit interactions and strong correlations. Figure 4 shows the results for the magnetic moment as a function of effective $U_{\rm eff}$ for four cases: AF/FM with and with out spin–orbital coupling, as well as comparison with the experimental value of 1.74 $\mu_{\rm B}$ [12]. It is evident that the magnetic moment depends on the effective Hubbard $U_{\rm eff}$ correction. Inspection of the local density of states (DOS) reveals occupation of the U 5f states by two electrons, which gives rise to a magnetic moment of 2.0 $\mu_{\rm B}$/U atom in the FM case for all $U_{\rm eff}$ values considered, and 1.9 $\mu_{\rm B}$/U atom in the AF case for $U_{\rm eff} \geqslant 1.5$ eV, both slightly larger than the experimental value (1.74 $\mu_{\rm B}$). Meanwhile, for $U_{\rm eff} \approx 1.0$ eV, the calculation gives a magnetic moment in good agreement with the experimental value for the AF ordering, but the FM ordering is more stable for this $U_{\rm eff}$ as shown in figure 2.

As can be seen in figure 4, a slightly lower magnetic moment results if spin–orbital coupling is included. A magnetic moment of 1.9 $\mu_{\rm B}$/U atom was calculated in the AF case for $U_{\rm eff} \geqslant 3.0$ eV. At the experimental magnetic moment, $U_{\rm eff}$ is about 2.0 eV for the AF case, but FM ordering is still more stable, as shown in figure 2, similar to the cases without the spin–orbital coupling.

UO_2 in the $Fm\bar{3}m$ phase is an AF insulator with a band gap of roughly 2 eV [8]. For $U_{\rm eff} = 0$ eV, the f band does not split for either the AF or the FM case and the obtained ground state is metallic, which disagrees with available experiments [8]. However, for nonzero $U_{\rm eff}$, the strong correlation for the 5f electrons of U atoms results in the removal of the degeneracy for 5f bands near the Fermi level (not shown here). The 5f bands split into two energy regions, one is mainly at the top of the valence states and the other is at the bottom of the conduction states, and the 2p orbitals of O predominate the lower valence states and partially hybridize with 5f orbitals of U at the top of the valence band, in turn leading to insulator characteristic and increasing the band gap as $U_{\rm eff}$ increases. In particular, the band gap for the AF phase is 1.2, 1.5 and 1.9 eV, corresponding to $U_{\rm eff}$ of 3.0, 3.5 and 4.0 eV, respectively.

We further investigated the Bader charge of the U ion in UO_2 as a function of the effective $U_{\rm eff}$ for the case of the AF configuration (figure 5). For $U_{\rm eff} \leqslant 3.0$ eV, the charge for the U ion increases almost linearly from 2.11 to 2.37. If we increase $U_{\rm eff}$ above 3.0 eV, the charge for the U ion fluctuates around 2.37. However, the value may change for U defects. For example, in the case of the U Frenkel pair, the charge for U interstitial has a value of 2.21.

Our results show that by choosing an appropriate U it is possible to consistently describe the structural properties of UO_2 for $U_{eff} \approx 3.0$ eV, if the optical properties are not the most important consideration. The corresponding bulk modulus is 195.4 GPa, in better agreement with the experimental value of 207 GPa [15], compared to a value of 180.7 GPa for $U_{eff} = 4.5$ eV. It is worth noting that the bulk modulus from the LDA + U approach [14] is a slight overestimation and the GGA+U approach here underestimates the value.

3.2. Phase transition

At high pressure UO_2 can transform to the high-pressure orthorhombic cotunnite-type structure ($Pnma$). Though it is well known that the cubic fluorite phase ($Fm\bar{3}m$) is the ground state structure of UO_2, it is important for the DFT+U approach to capture such features correctly. Our results indicate that the $Fm\bar{3}m$ phase is more stable than the $Pnma$ phase, and the magnitude of the lattice energy for the AF fluorite structure is 1.2 eV per unit cell (U_4O_8) lower than that of the cotunnite phase using the GGA + U formalism for U_{eff} between 2.5 eV and 4.5 eV. However, for $U_{eff} = 0$ eV, the energy difference between AF $Pnma$ and AF $Fm\bar{3}m$ phases is 1.8 eV, while the corresponding energy difference between the FM phases is 2.3 eV.

As one might expect, the equilibrium volume depends on the parameter U_{eff} and increases almost linearly with U_{eff} for both phases. In fact, for $U_{eff} = 3.0$ eV, GGA + U gives a slight overestimation of the lattice parameter for both phases. After full relaxation of all internal coordinates and cell shape, the optimized volume of the $Pnma$ phase is 156.47 Å^3 (a = 6.08 Å, b = 3.62 Å and c = 7.11 Å) per unit cell, while the volume for the fluorite phase is 168.75 Å^3. Thus, the calculated volume reduction is 7.3%, which is in good agreement with the experimental value of 7% [15].

We also investigated the phase transition from $Fm\bar{3}m$ to $Pnma$. The results of the total lattice energy as a function of unit-cell volume is shown in figure 6. Corresponding to hydrostatic conditions from the slope of the common tangent rule, the calculated phase transition pressure is 20.0 and 19.1 GPa for the case of $U_{eff} = 3.0$ and 4.0 eV, respectively. Although these values are smaller than the experimental value of 42 GPa [15], they are in much better agreement with experiment than the LDA + U value of 7.8 GPa [14]. These smaller values are due to the fact that the total lattice energy of the $Fm\bar{3}m$ phase is more significantly influenced than that of the $Pnma$ phase as the parameter U_{eff} increases. Consequently an even better agreement with the experimental phase transition pressure is expected if $U_{eff} = 0.0$ eV is used, due to the larger energy difference, but its use would give a poorer representation of other materials properties of interest discussed above.

In order to understand and control the fundamental solid state processes that govern the phase transition, direct mapping of the electrostatic potential distribution is highly desirable for both phases. The phase transition involves the displacement of atoms from one lattice site to another, and

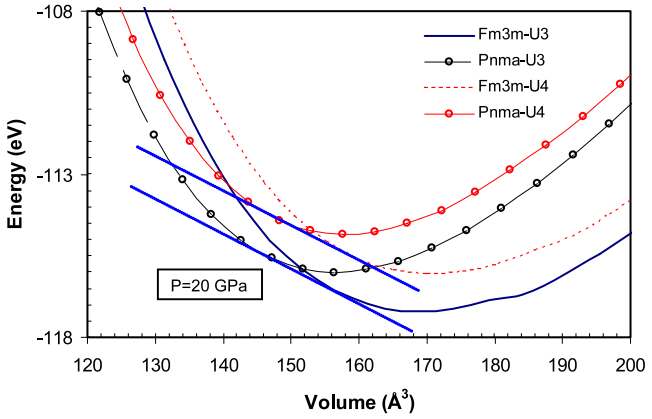

Figure 6. Energy versus volume curve for $Fm\bar{3}m$ and $Pnma$ phases of UO_2.

hence a microscopically tailored electrostatic potential. Here we present the local electrostatic potential for both $Fm\bar{3}m$ and $Pnma$ structures by obtaining the redistribution of the local electrostatic potential along the z-direction (vertical) and x/y direction (lateral). As can be seen in figure 7(A), the local electrostatic potentials along both vertical and lateral directions are almost identical for the $Fm\bar{3}m$ phase. However, the $Pnma$ phase exhibited a variation in the local electrostatic potential different from the $Fm\bar{3}m$ phase. In fact, as shown in figures 7(B)–(D), the distribution of the local electrostatic potential is not isotropic. This implies that an externally applied anisotropic stress can be used to modify this electrostatic landscape more easily from the $Fm\bar{3}m$ phase than under hydrostatic conditions. Thus, the phase transition pressure for UO_2 can be less than 42 GPa under reactor operating conditions.

3.3. Atomization and heat of formation energies

At zero temperature, the heat of formation ΔH_f of bulk UO_2 is defined as

$$\Delta H_f = E_{tot}^{UO_2} - E_{tot}^{\alpha-U} - E_{tot}^{O_2} = E_{at}^{\alpha-U} + E_{at}^{O_2} - E_{at}^{UO_2}, \quad (1)$$

where E_{tot} is the total energy of the systems and E_{at} is the atomization energy.

We first calculated the atomization (cohesive) energies of the oxygen molecule and uranium metal because these elemental reference energies are needed to calculate the heat of formation energy of uranium oxide as well as the defect formation energies (enthalpies). The spin-polarized total energy of the free O and U atoms are −1.86 eV and −4.45 eV, respectively. Zero-point vibrational energy contributions are not included here. For the O_2 molecule, the atomization energy E_{at} and the equilibrium bond length r_{eq} are listed in table 1. Our calculation gives the equilibrium bond length r_{eq} to be 1.22 Å, in agreement with experimental values [27, 28] and previous PAW calculations [13, 29]. Meanwhile, our calculation yields a total energy of −9.95 eV/O_2, which corresponds to the atomization energy of 6.23 eV/O_2, leading to an overestimate of about 0.5 eV/atom compared with

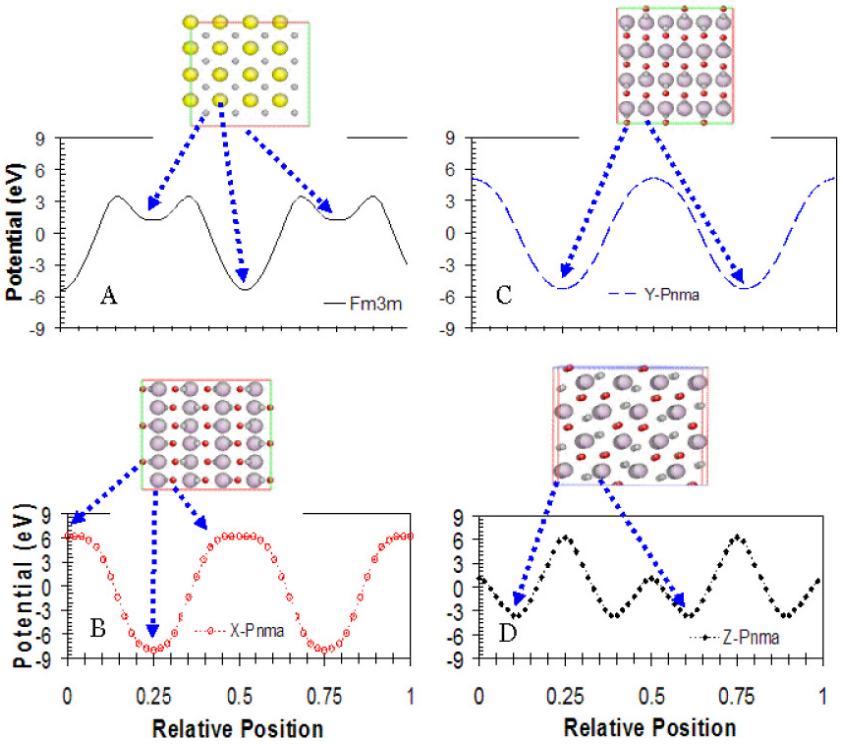

Figure 7. Local static electronic potential energy along directions of x, y and z.

Table 1. Lattice constants of uranium metal in the orthorhombic α-phase structure calculated for different U_{eff}, and bond length of the O_2 molecule, total and atomization energies per U atom and per O_2 molecule, compared to the results of experiments.

	α-U metal					
	U_{eff} (eV)				O_2	
	0	0.5	3.0	Expt.[a]		Expt.[b]
a (Å)	2.804	2.834	3.313	2.836	1.22	1.21
b (Å)	5.867	5.881	5.863	5.867		
c (Å)	4.903	4.928	5.667	4.936		
E (eV)	−11.15	−10.57	−8.4		−9.95	
E_{at} (eV)	6.70	6.12	3.95		6.23	5.25

[a] Reference [35].
[b] Reference [27, 28].

the experimental value of 5.25 eV/O_2 [27, 28]. However, this result is in excellent agreement with other DFT–GGA studies [13, 29]. When comparing our calculated results with previous DFT calculations for the UO_2 system, an underestimation of the binding energy is common. For example, Geng *et al* [30] estimated that the O_2 over binding is only about 0.3 eV/atom with GGA, which means that O_2 is not in the ground state. Such underestimation of the binding energy of the oxygen molecule tends to make the heat of formation energy of UO_2 more exothermic.

Experimentally, pure uranium metal is weakly to moderately correlated [31], i.e. f-electron correlation effects presented in the orthorhombic α-phase (α-U) are not as strong as in its oxide. Thus, the appropriate values for the effective Hubbard parameter U_{eff} should be different for the UO_2 system and the metallic phase. Here we investigate the property dependence of α-U on U_{eff}. Table 1 lists the calculated lattice constants of uranium metal in the orthorhombic α-phase structure, and total and atomization energies per U atom, for U_{eff} values of 0, 0.5 and 3.0 eV, respectively, along with the results of experiments. Among three possibilities for the magnetic states studied—nonmagnetic (NM), AF and FM—only the results for the most stable state are listed. It is found that the most stable state is NM for U_{eff} of 0 and 0.5 eV, and AF for U_{eff} of 3.0 eV. As for $U_{\text{eff}} = 3.0$ eV, the total energy of U in α-uranium metal is −8.4 eV/atom, corresponding to the cohesive energy of 3.95 eV/atom. As can be seen, $U_{\text{eff}} = 0.5$ eV reproduces the experimental data very well, and such a value is also consistent with the recommendation of Chantis *et al* [32].

We now turn our attention to UO_2. The lattice parameters for UO_2 in the AF fluorite structure calculated by the GGA+U method are $a = 5.544$ Å and $c = 5.490$ Å, which compare very well with the experimental value [33] of $a = 5.468$ Å as listed in table 2. The lattice parameter in general increases as U_{eff} increases for UO_2, and such behaviour is due to a slight hybridization of U 5f and O 2p orbitals. However, after full relaxation of the supercell, only the FM structure can maintain the cubic lattice with or without spin–orbital coupling, and the AF structure turns to the tetragonal symmetry ($a = b \neq c$) due to the antiferromagnetic ordering along the c-axis [19]. The cohesive energy as listed in table 2 is about 22.98 and 21.16 eV/UO_2, corresponding to U_{eff} of 0 and 3.0 eV, respectively, both qualitatively agreeing with the experimental value of 22.31 eV/UO_2 [34].

Table 2 also lists the results for the heat of formation energy for U_{eff} values of 0 and 3.0 eV, as well as comparison

Table 2. Properties of UO_2. Lattice constants, total energy, cohesive energy and the heat of formation energy of UO_2 for different U_{eff}, compared to experimental data. Given $U_{eff} = 3.0$ eV for UO_2, the formation energy is −8.228, −8.806 and −10.978 eV/UO_2 when the U_{eff} for the metal is 0, 0.5 and 3.0 eV, respectively.

		U_{eff} (eV)		
		0	3.0	Expt.[a]
a	(Å)	5.423	5.544	5.468
c	(Å)	5.423	5.490	
E_{tot}	(eV/UO_2)	−31.143	−29.325	
E_{coh}	(eV/UO_2)	22.979	21.161	22.31
ΔE_h	(eV/UO_2)	−10.046	−8.228	
			−8.806	
			−10.978	

[a] Reference [33, 34].

Table 3. Intrinsic defect formation energy (eV) in UO_2.

	$U_{eff} = 0.5$ (eV)		$U_{eff} = 3.0$ (eV)		
	U-rich	O-rich	U-rich	O-rich	Expt.[a]
O_I	1.96	−2.44	3.05	−2.44	
O_V	0.66	5.06	−0.43	5.06	
U_I	4.67	13.48	2.50	13.48	
U_V	2.30	−6.50	4.48	−6.50	
O_{FP}^{∞}	2.61	2.61	2.61	2.61	3.0–4.6
O_{FP}	0.07	0.07	0.07	0.07	
U_{FP}^{∞}	6.974	6.974	6.974	6.974	9.5
U_{FP}	6.968	6.968	6.968	6.968	
Sch^{∞}	3.62	3.62	3.62	3.62	6.0–7.0
Sch⟨111⟩	0.01	0.01	0.01	0.01	
Sch⟨110⟩	0.04	0.04	0.04	0.04	
Sch⟨100⟩	0.65	0.65	0.65	0.65	

[a] Reference [33].

with experimental values. In the case without the effective Hubbard U_{eff} correction ($U_{eff} = 0$ eV), our calculation gives a formation energy of $\Delta H_f = -10.046$ eV/UO_2. As $U_{eff} = 3.0$ eV for UO_2, the formation energy is −8.228, −8.806 and −10.978 eV/UO_2 when the U_{eff} for the metal is 0, 0.5 and 3.0 eV, respectively. This clearly indicates that the heat of formation depends strongly on the level of the effective Hubbard U_{eff} correction. In fact there exists an additional complication with the DFT+U method, as pointed out by Lany and Zunger [6]. The appropriate U_{eff} value for the U f states should be smaller in the metallic state than in the ionic UO_2 with stronger screening effects, but in practice only energies calculated with the same value for U_{eff} were applied [20], in general leading to an underestimation of the metallic elemental reference energies, i.e. metal chemical potential in GGA + U calculations. Such underestimation also tends to make the heat of formation energy of UO_2 more exothermic. We recommend using a different value of the effective Hubbard U_{eff} for the ionic insulator and the metal, corresponding to 3.0 eV and 0.5 eV, respectively.

3.4. Intrinsic and extrinsic defect formation energies

According to the formalism of Van de Walle and Neugebauer [4], the defect formation energy ΔE_f (E_F, D^q) of a defect D in charge state q is calculated as function of the Fermi level E_F

$$\Delta E_f = E_{D,q} - E_{perf} - \sum_i n_i \mu_i + q(E_v + E_F + \Delta V), \quad (2)$$

where $E_{D,q}$ and E_{perf} are the total energies of a solid supercell with and without defect D, respectively. μ_i is the chemical potential of atomic species i, and n_i is the number of defect atoms of element i removed (negative n_i) or added (positive n_i) to create the defect. E_v represents the energy at the valence band maximum (VBM) in the perfect crystal and E_F is the Fermi energy relative to E_v. The use of E_v as a reference for the zero of potential has no effect on the accuracy of the calculated charge neutral defect formation energies. Related to the finite-size error, the term ΔV represents the electrostatic potential correction determined by inspecting the potential in the supercell far from the impurity and aligning it with the electrostatic potential in the perfect crystal [4].

As shown in equation (2), the formation energy of a charge neutral defect depends on the oxygen chemical potential μ_O and uranium chemical potential μ_U. The chemical potential comes from how the environmental condition is determined. In fact, the upper limit on μ_O (under O-rich conditions) is given by $\mu_O = \mu_{O[O_2]}$, i.e. the energy of O in a O_2 molecule being −4.975 eV. Although the standard form of DFT yields only zero-temperature total energies, the chemical potential of the O_2 molecule can be related to temperature T and partial pressure P using standard thermodynamic expressions.

The upper limit on μ_U (under U-rich conditions) is determined by $\mu_U = \mu_{U[\alpha-U]}$, i.e. the energy of U in α-uranium metal with $U_{eff} = 3.0$ eV being 8.4 eV/atom. In addition to the upper limits defined above, according to

$$\mu_U + 2\mu_O = \mu_{tot}[UO_2] = \Delta H_f + \mu_{U[\alpha-U]} + 2\mu_{O[O_2]}, \quad (3)$$

where μ_{tot} [UO_2] is the total energy of a three-atom unit of the bulk UO_2, the lower limit, μ_O^{min}, may be written as

$$\mu_O^{min} = \tfrac{1}{2}[\mu_{tot}[UO_2] - \mu_{U[\alpha-U]}] \quad (4)$$

for O ions and

$$\mu_U^{min} = [\mu_{tot}[UO_2] - 2\mu_{O[O_2]}] \quad (5)$$

for U ions. Due to the large value of the heat of formation ΔH_f (∼−9 eV), the ranges of μ_O and μ_U are wide and the specific experimental conditions cannot be determined without further considerations.

Table 3 lists the results of formation energies of intrinsic point defects using GGA + U for $U_{eff} = 3.0$ eV for UO_2 and $U_{eff} = 0.5$ eV for α-U under O-rich and O-poor conditions, as well as the results for $U_{eff} = 3.0$ eV for both UO_2 and α-U. For the two studied magnetic states, AF and FM, only the results for the most stable state are listed. It is interesting to note that FM phases are more stable. The formation energy for point defects (O and U vacancy and interstitial: O_V, U_V, O_I, and U_I) strongly depends on whether the environment condition is O-rich/U-poor or O-poor/U-rich. This is related to the fact

that the chemical potential and the choice of U_{eff} for α-U give rise to differences in the heat of formation. For example, the preferred type of O defect predicted by this study is interstitial and vacancy under O-rich and O-poor conditions, respectively. In the case of $U_{\text{eff}} = 3.0$ eV for α-U, the energetically favoured type of U defect is interstitial and vacancy under O-poor and O-rich conditions, respectively. However, it is predicted that the U vacancy is the energetically favoured U defect regardless of whether the condition is O-poor or O-rich in the case of $U_{\text{eff}} = 0.5$ eV for α-U. The energy ranking of these point defects is also changed from $O_V < U_I < O_I < U_V$ to $O_V < O_I < U_V < U_I$ as U_{eff} decreases from 3.0 to 0.5 eV for α-U. In fact, equilibrium conditions under typical operating conditions in which T is around 1000 K may be considered to be close to neither the O-rich limit nor the O-poor limit.

To compare more directly with experimental data, table 3 also lists the formation energies of complex intrinsic defects, i.e. Frenkel pairs (FP) for O and U and Schottky defects (Sch). It is convenient to envisage that the complex defects are formed by the point defects that are isolated and non-interacting with one another. The corresponding formation energy is just the sum of the formation energies of point defects. The results are also listed in tables 3 indicated as OFP^{∞}, UFP^{∞} and Sch^{∞}. As listed in table 3, the formation energies for the complex defects do not depend on whether the experiment is under O-poor condition or O-rich condition and which U_{eff} is chosen for α-U. The results in all cases for unbound complex defects are calculated to be 2.61 eV, 6.97 eV and 3.62 eV for OFP^{∞}, UFP^{∞} and Sch^{∞}, respectively, which are lower than the experimental data (corresponding to 3.0–4.6 eV, 9.5 eV and 6.0–7.0 eV, respectively) [33] and previous DFT results [16–20]. The large values from previous DFT results [16–20] are mainly due to the fact that only one magnetic state was studied, which prevents exploration of lower energy states. Furthermore, as pointed by Hine *et al* [5], if the atoms far from a charged defect are prevented from relaxing in response to the long-ranged elastic and electrostatic interactions, the defect formation energy is overestimated. For example, in the case for UFP, if all atoms are allowed to relax, the formation energy is reduced to 6.8 eV. Nevertheless, our calculations are aligned with previous suggestions from experiment [33] and theory [16–20] and the energy ranking of these complex defects is OFP < Sch < UFP.

Another situation was also considered, in which defects are bound closely. There are three types of Schottky defects in which the uranium vacancy sits in the centre of oxygen cage, and two oxygen vacancies are aligned in ⟨100⟩, ⟨110⟩ and ⟨111⟩ directions, respectively. Again, FM phases are more energetically favourable in all cases. The results are also listed in table 3. It is interesting to note that the association energy, the difference in formation energy between bound UFP and unbound UFP, is less than 0.01 eV. However, the formation energies for bound OFP and Schottky are reduced significantly compared with unbound cases, which indicate that the association energy plays a role for bound OFPs and Schottky defects.

To model Xe in the fuel, it is convenient to envisage that Xe is trapped in a specific site with two steps: defect formation and Xe incorporation corresponding to insertion of an extrinsic defect into an intrinsic defect site. Six possible Xe trapping sites are studied: octahedral interstitial site (O_{IS}), O_V, U_V, OFP, UFP and Schottky. The corresponding formation and incorporation energies are E^F and E^I, respectively. There is no energy required to create the O_{IS}, and the values of E^F for others are listed in table 3 discussed above. Our study indicates that as Xe is embedded into the host of UO_2, the FM phase is more energetically favourable in all cases. The values of E^I are listed in table 4. In contrast to the OFPs being the dominant complex defect, it is most likely that the Xe atom is trapped by the Schottky site, corresponding to the incorporation energy of 2.9 eV. The existence of the neutral trivacancies, i.e. a Schottky trio as a trap for Xe in UO_2, is consistent with experimental data [21]. Furthermore, the incorporation energies are positive in all cases and it clearly indicates that xenon is strongly unstable in the UO_2 system [23]. In the cases of O_{IS}, O_V and U_V as the Xe trapped site, the incorporation energies from our calculations are 8.07, 9.01 and 5.18 eV, respectively, significantly lower than previous DFT calculations [23] which reported 11.2, 9.4 and 13.9 eV, respectively. Such significantly high incorporation energies from previous DFT calculations [23] can be attributed to the use of a smaller supercell containing only 12 atoms, as well as the effect of magnetic ordering in which only one magnetic state was investigated. We note that the incorporation energy may be further reduced if in the process of relaxing the host atoms around the defect, the volume of the supercell is relaxed as well. However, such volume relaxation would actually correspond to an ordered array of impurities at very high concentration and could result in a very different lattice constant [4].

Table 4. Incorporation energies of Xe at six different sites.

Xe site	O_{IS}	O_V	U_V	O_{FP}	U_{FP}	Sch
E^I (eV)	8.07	9.01	5.18	8.91	3.83	2.90

In order to investigate the effect of possible swelling in the fuel, the supercells containing Xe were further optimized in which all the atoms, cell shape and cell volume were allowed to relax. In most cases, the energy gained was under 0.2 eV, but for O_V it was 1.8 eV. Thus the conclusion that Xe prefers to be trapped by a Schottky site is still valid after full volume relaxation. The volume swelling is about 2.4%, 2.8%, 0.6%, 2.9%, 3.6% and 1.5%, corresponding to the Xe trapping sites of O_{IS}, O_V, U_V, OFP, UFP and Schottky, respectively. It is interesting to note that Xe trapped by a U vacancy has the lowest volume expansion and that by UFP the highest. In contrast, previous DFT calculations [23], with only a 12-atom supercell, predicted a dramatic volume expansion, i.e. 68%, 78% and 41% for O_{IS}, O_V and U_V, respectively.

4. Conclusions

Intrinsic and extrinsic defect properties and the pressure-induced phase transition of UO_2 have been studied using first principles by the all-electron projector-augmented-wave

(PAW) method. An antiferromagnetic insulating ground state was obtained for $U_{\text{eff}} \geqslant 2.0$ eV with the GGA + U formalism, which is consistent with experiment. By systematically studying the effect of U_{eff}, the present study shows that $U_{\text{eff}} = 3.0$ eV is most suitable for a consistent description of structural properties of UO_2 and modelling of phase transition processes. The phase transition pressure for UO_2 is about 20 GPa. Our results for the formation energies of intrinsic defects reveal large variations in the calculated values depending on the chemical potential and the environmental conditions (O-rich/O-poor). The results for extrinsic defects were consistent with experimental data in that Xe prefers to be trapped by the Schottky site.

Acknowledgments

We acknowledge useful discussions with Fei Gao. This work was funded by the Materials Sciences and Engineering Division, Office of Basic Energy Sciences (BES), US Department of Energy (DOE) under contract no. DE-AC05-76RL01830 under the Computational Materials Science Network. The computations were performed using resources of the National Energy Research Scientific Computing Center, which is supported by the Office of Science of the DOE under contract no. DE-AC02-05CH1123, and the MSCF in EMSL, a national scientific user facility sponsored by the US DOE, Office of Biological and Environmental Research and located at Pacific Northwest National Laboratory. RD was partly supported by a Nuclear Energy Advanced Modeling and Simulation project.

References

[1] Burns P C and Finch R 1999 *Uranium: Mineralogy, Geochemistry and the Environment* ed P H Ribbe (Washington, DC: The Mineralogical Society of America)
[2] Matzke H and Kinoshita M 1997 Polygonization and high burnup structure in nuclear fuels *J. Nucl. Mater.* **247** 108–15
[3] Kohn W and Sham L J 1965 Self-consistent equations including exchange and correlation effects *Phys. Rev.* **140** A1133
[4] Van de Walle C G and Neugebauer J 2004 First-principles calculations for defects and impurities: applications to III-nitrides *J. Appl. Phys.* **95** 3851–79
[5] Hine N D M, Frensch K, Foulkes W M C and Finnis M W 2009 Supercell size scaling of density functional theory formation energies of charged defects *Phys. Rev.* B **79** 024112
[6] Lany S and Zunger A 2008 Assessment of correction methods for the band-gap problem and for finite-size effects in supercell defect calculations: case studies for ZnO and GaAs *Phys. Rev.* B **78** 235104
[7] Perdew J P, Chevary J A, Vosko S H, Jackson K A, Pederson M R, Singh D J and Fiolhais C 1992 Atoms, molecules, solids, and surfaces: applications of the generalized gradient approximation for exchange and correlation *Phys. Rev.* B **46** 6671
[8] Baer Y and Schoenes J 1980 Electronic-structure and coulomb correlation-energy in UO_2 single-crystal *Solid State Commun.* **33** 885–8
[9] Dudarev S L, Botton G A, Savrasov S Y, Humphreys C J and Sutton A P 1998 Electron-energy-loss spectra and the structural stability of nickel oxide: an LSDA + U study *Phys. Rev.* B **57** 1505–9
[10] Dudarev S L, Botton G A, Savrasov S Y, Szotek Z, Temmerman W M and Sutton A P 1998 Electronic structure and elastic properties of strongly correlated metal oxides from first principles: LSDA + U, SIC-LSDA and EELS study of UO_2 and NiO *Phys. Status Solidi* a **166** 429–43
[11] Kudin K N, Scuseria G E and Martin R L 2002 Hybrid density-functional theory and the insulating gap of UO_2 *Phys. Rev. Lett.* **89** 266402
[12] Faber J and Lander G H 1976 Neutron-diffraction study of UO_2—antiferromagnetic state *Phys. Rev.* B **14** 1151–64
[13] Da Silva J L F, Ganduglia-Pirovano M V, Sauer J, Bayer V and Kresse G 2007 Hybrid functionals applied to rare-earth oxides: the example of ceria *Phys. Rev.* B **75** 045121
[14] Geng H Y, Chen Y, Kaneta Y and Kinoshita M 2007 Structural behavior of uranium dioxide under pressure by LSDA + U calculations *Phys. Rev.* B **75** 054111
[15] Idiri M, Le Bihan T, Heathman S and Rebizant J 2004 Behavior of actinide dioxides under pressure: UO_2 and ThO_2 *Phys. Rev.* B **70** 014113
[16] Crocombette J P, Jollet F, Nga L T and Petit T 2001 Plane-wave pseudopotential study of point defects in uranium dioxide *Phys. Rev.* B **64** 104107
[17] Freyss M, Petit T and Crocombette J-P 2005 Point defects in uranium dioxide: *ab initio* pseudopotential approach in the generalized gradient approximation *J. Nucl. Mater.* **347** 44–51
[18] Gupta F, Brillant G and Pasturel A 2007 Correlation effects and energetics of point defects in uranium dioxide: a first principle investigation *Phil. Mag.* **87** 2561–9
[19] Iwasawa M, Chen Y, Kaneta Y, Ohnuma T, Geng H Y and Kinoshita M 2006 First-principles calculation of point defects in uranium dioxide *Mater. Trans.* **47** 2651–7
[20] Nerikar P, Watanabe T, Tulenko J S, Phillpot S R and Sinnott S B 2009 Energetics of intrinsic point defects in uranium dioxide from electronic-structure calculations *J. Nucl. Mater.* **384** 61–9
[21] Matzke H 1980 Gas-release mechanisms in UO_2—a critical-review *Radiat. Eff. Defects Solids* **53** 219–42
[22] Olander D R and Wongsawaeng D 2006 Re-solution of fission gas–a review: Part I. Intragranular bubbles *J. Nucl. Mater.* **354** 94–109
[23] Freyss M, Vergnet N and Petit T 2006 *Ab initio* modeling of the behavior of helium and xenon in actinide dioxide nuclear fuels *J. Nucl. Mater.* **352** 144–50
[24] Blochl P E 1994 Projector augmented-wave method *Phys. Rev.* B **50** 17953–79
[25] Kresse G and Furthmuller J 1996 Efficient iterative schemes for *ab initio* total-energy calculations using a plane-wave basis set *Phys. Rev.* B **54** 11169–86
[26] Kresse G and Hafner J 1993 *Ab initio* molecular-dynamics for liquid-metals *Phys. Rev.* B **47** 558–61
[27] Herzberg G 1989 *Molecular Spectra and Molecular Structure I. Spectra of Diatomic Molecules* 2nd edn (Malabar, FL: Krieger)
[28] Huber K and Herzberg G 1979 *Molecular Spectra and Molecular Structure: IV. Constants of Diatomic Molecules* (New York: Van Nostrand-Reinhold)
[29] Jomard G, Amadon B, Bottin F and Torrent M 2008 Structural, thermodynamic, and electronic properties of plutonium oxides from first principles *Phys. Rev.* B **78** 075125
[30] Geng H Y, Chen Y, Kaneta Y, Iwasawa M, Ohnuma T and Kinoshita M 2008 Point defects and clustering in uranium dioxide by LSDA + U calculations *Phys. Rev.* B **77** 104120
[31] Lander G H, Fisher E S and Bader S D 1994 The solid-state properties of uranium A historical perspective and review *Adv. Phys.* **43** 1–111

[32] Chantis A N, Albers R C, Jones M D, van Schilfgaarde M and Kotani T 2008 Many-body electronic structure of metallic alpha-uranium *Phys. Rev.* B **78** 081101

[33] Matzke H 1987 Atomic transport-properties in UO_2 and mixed oxides (U, PU)O_2 *J. Chem. Soc. Faraday Trans.* II **83** 1121

[34] Brooks M S S and Kelly P J 1983 On the cohesive energy and charge–density of uranium-dioxide *Solid State Commun.* **45** 689–92

[35] Barrett C S, Mueller M H and Hitterman R L 1963 Crystal structure variations in alpha uranium at low temperatures *Phys. Rev.* **129** 625